Information Sciences Letters
An International Journal

http://dx.doi.org/10.18576/isl/120110

Effect of Triple Treatment on the Surface Structure and Hardness of 304 Austenitic Stainless Steel

Mohammed H. Fawey[1,], A. M. Abd El-Rahman[1,2], F. M. El-Hossary[1] and Tawheed Hashem[3]*

[1]Physics Department, Faculty of Science, Sohag University, 82524 Sohag, Egypt
[2]Physics Department, King Abdulaziz University, Jeddah 21589, Kingdom of Saudi Arabia
[3]Institute of Functional Interfaces (IFG), KIT-Innovation HUB, Karlsruhe Institute of Technology (KIT), Hermann-von Helmholtz-Platz 1, 76344 Eggenstein-Leopoldshafen, Germany

Received: 2 Jun. 2022, Revised: 21 Jul. 2022, Accepted: 8 Aug. 2022.
Published online: 1 Jan. 2023.

Abstract: Nitriding, annealing, and carbonitriding processes are conducted to modify the surface of AISI 304 austenitic stainless steel via radio frequency plasma. A ~20 μm thick nitride layer is obtained in ten minutes at a plasma power of 450 W. Hence, all nitrided samples are annealed under vacuum for one hour at 400 ˚C. The nitrided-annealed samples are carbonitrided via the identical technique at various C_2H_2/N_2 gas pressure ratios. Numerous analytical techniques, including X-ray diffractometry, glow discharge optical spectroscopy (GDOS), Talysurf Intra Profilemeter, optical microscopy (OM), scanning electron microscopy (SEM), and Vickers microhardness tester, were employed to investigate the triple-treated specimens. Microstructure analysis of the triple-treated samples reveals the formation of N_2 expanded austenite phase (γ_N), γ′-Fe_4N, CrN, Fe_3C, and Fe_7C_3. The results indicate that the elemental composition, microhardness, and thickness of the triple-treated layers are all depending on the gas composition. After carbonitriding, the total thickness of the compound layer grew from ~20 to ~34.5 μm. The surface microhardness of the triple-treated samples increased as the C_2H_2/N_2 gas composition ratio increased up to 70%, reaching 1,497±33.5 HV0.1, which is ~6.8 and ~1.42 folds higher than the untreated and prenitrided samples, respectively.

Keywords: Nitriding; Carbonitriding; Annealing; Glow discharge optical spectroscopy; Microhardness; Surface morphology.

1 Introduction

Due to the formation of an intrinsic and self-healing passive coating, principally composed of chromium oxide, austenitic stainless steels (ASSs) of AISI 316 and AISI 304 are widely renowned for their remarkable corrosion resistance [1,2]. As a result, they are widely used in a variety of current industrial production sectors, including food and chemical processing, biomedical, petrochemical, automotive, and nuclear [1,3,4,5]. However, their limited mechanical properties, like surface microhardness and wear resistance, limit their application range. To improve their mechanical properties and hereafter enlarge their applications, surface modification is required to achieve a surface layer of a favorite microstructure without touching the bulk properties. Plasma immersion ion implantation (PIII) [6], microwave-induced N_2 plasma [7], plasma spraying method [8], RF plasma nitriding [9], RF plasma carbonitriding [10], and duplex treatment [11,12] are a few of the most recent innovative procedures developed to enhance the microhardness and wear resistance of ASS. Carburizing, nitriding, and carbonitriding have been used as single surface treatment techniques for a long time [13,14,15]. Nitriding is a well-established thermochemical treatment based on inserting N_2 atoms into an ASS matrix, forming a thick modified surface layer of supersaturated N_2 solid-solution fcc phase [16]. Two sub-layers of this modified surface layer can be identified: a compound layer composed of iron nitrides Fe_4N and/or $Fe_{2-3}N$ to boost tribological characteristics and corrosion resistance [17], followed by a diffusion layer of MN nitride precipitation (M = Cr, Mo, V,.....) to provide wear resistance and fatigue resistance [18]. Microstructure and composition of the formed compound and diffusion layers are affected by the nitriding conditions, such as temperature and gas composition. Nitriding of ASSs can greatly increase their surface hardness and wear resistance, but it is not without drawbacks. Unfortunately, it is typically characterized by precipitation of chromium nitride, which results in a noteworthy decrease in the corrosion resistance of the nitrided surface

*Corresponding author e-mail: mohammed.fawey@gmail.com

[19,20]. This has led to recent research into using low nitriding temperatures of less than 450 ˚C [21] to increase the corrosion resistance of nitrided ASSs rather than the more common temperature of around 600 ˚C. High surface microhardness and excellent corrosion resistance have been achieved by plasma nitriding of ASS at low temperatures [22]. In gas nitriding [23] and PIII at temperatures between 350 and 450 ˚C [24], this effect has been seen. Alternatively, applying a carbonitriding process to ASSs is an effective thermochemical surface treatment for improving their wear resistance. In addition, the structure of a carbonitrided layer also comprises compound and diffusion zones. Carbonitrides phases with a high concentration of C and N_2 are formed on the sample surface to create a compound zone. Underneath the compound layer lies the diffusion zone, which is a strong arrangement of N_2 and C. The diffusion zone tends to be thicker than the compound layer that has a few microns thick [25]. The corrosion resistance of the carbonitrided ASS specimens is higher than that of the specimens treated solely by nitriding or carburizing. An explanation for this is that γ_N [26] is formed, which has superior corrosion resistance in comparison to the γ-austenite phase [27]. Moreover, the nitride and carbide phases in the presence of the γ_N and C expanded austenite phase (γ_C) phases improve the surface microhardness [28].

On the other hand, a duplex plasma treatment has been established to further improve the stainless steel's mechanical, tribological, and corrosion properties [11,12]. Duplex treatment is a surface modification technique combining two consecutive actions of, a hard coating on a treated surface. To sustenance the coating without plastic deformation, the specimen must have appropriate hardness and flow strength. Plasma nitriding/plasma carbonitriding [11], plasma nitriding/TiN deposition [12], plasma nitriding/DLC film deposition [29], plasma carbonitriding/post-oxidation [30], plasma nitriding/TiN coating [31], and plasma nitriding/plasma nitriding–oxidizing [32] have all been successfully applied to enhance the properties of ASSs surfaces.

Above and beyond, ASS pretreatment, such as heat treatment, cold working, and alloying, is well-known to have a significant impact on its qualities [33]. Heat treatment could be essential to decrease porosity, release the residual stress, and/or improve further coating properties [34]. Typically, the strength and stress levels of the material can be controlled by alloying and cold working process, while the microstructure and grain size, and consequently the diffusivity, are impacted by heat treatment. For instance, Jiaxin Zhang et al. studied the microstructure and tensile characteristics of metastable ASSs after annealing for 2 h [35]. Next annealing at 800 ˚C to 950 ˚C, the main size of the reversed austenite grains was reduced to around 2.3 − 4.8 μm, while the grain size grew to roughly 16 μm later annealing at 1000 ˚C. The grain growth is mostly due to the degradation increasing of carbide particles through the increasing of annealing temperature. Furthermore, they found that grain refinement boosted the yield and ultimate tensile strengths at the low annealing temperature. The purpose of the current work is to examine the microstructure and microhardness of AISI 304 ASS after a triple treatment (nitriding, annealing, and carbonitriding). The elemental composition, surface morphology, X-sectional morphology, phase distribution, and surface microhardness of the triple-treated AISI 304 ASS samples were investigated.

2 Methodologies

AISI 304 ASS sheet, 1 mm thick, was cut into 20 mm × 10 mm coupons. Its chemical composition is 69.95 wt.% Fe, 19.1 wt.% Cr, 8.5 wt.% Ni, 1.2 wt.% Mn, 0.5 wt.% Si, and 0.075 wt.% C. Acetone was used to clean the specimens before they entered the reactor quartz tube. An inductively coupled plasma was used to conduct nitriding and carbonitriding processes. The nitride AISI 304 ASS samples were annealed after nitriding and before carbonitriding. Fig. 1 reveals the schematic diagram of the RF plasma system that comprises a 50 cm long quartz reactor tube with a diameter of 4.15 cm. First, the reactor tube was evacuated to a 6×10^{-3} mbar base pressure using a rotary pump. A 13.56 MHz RF generator connected to an impedance matching network powered a copper induction coil with three turns to generate the discharge. The lower turn of the RF coil is fixed at a distance of 2.9 cm far away from the specimen surface. The water-cooling rate was set to 1500 cm^3/min for the substrate sample holder. During the nitriding process, the pure N_2 gas was used to increase the gas pressure in the quartz reactor tube from 7×10^{-3} mbar to roughly 8×10^{-2} mbar. Hence, the samples were subjected to a 10 min plasma treatment with a 450 W plasma input power. A thermocouple of Chromel-Alumel was used to measure the temperature of the specimen surface during the plasma nitriding. It was found that the nitriding process temperature remained relatively constant at around 450 ˚C. Finally, the nitrided specimen was kept inside the reactor tube for 15 minutes to cool down to room temperature (RT).

After this prenitrided process, the nitrided samples were annealed for one hour at 400 ˚C in a silica cylindrical tube under a vacuum of approximately 10^{-3} mbar. The annealed specimens were kept in the silica cylinder under vacuum in order to cool to RT. The specimens that had previously been nitrided and, hence, annealed were carbonitrided at various partial pressure ratios of C_2H_2, ranging from 10% to 70%, using the same technique, while the balance was pure nitrogen. The total pressure of gas was set at 8×10^{-2} mbar for carbonitriding. The distance between the lower turn of the RF coil and the specimen surface reduced to roughly 2.4 cm, while the substrate water cooling rate was decreased to 600 cm^3/min.

Carbonitriding of nitrided-annealed materials was carried out under identical plasma conditions (450 W plasma-power and 10 min plasma processing time). The specimen temperature was measured during the plasma carbonitriding. As the C_2H_2 pressure ratio is increased to 70%, the specimen temperature rises from 520 ˚C to 590 ˚C. At the end of the operation, the carbonitrided specimens were kept in the evacuated quartz tube till they cooled down to RT.

To determine the thickness of the treated layers, tiny workpieces were cut from the treated samples using an ISOMET low-speed saw. The X-sectioned specimens were mounted in an epoxy matrix using the cold-mounting procedure. Silicon-carbide abrasive grit of various grades (ranging from 40 to 400 meshes) was used in a series of processes to grind out the X-sections of the material. The X-sections were then refined to a mirror finish via micro-polish suspensions of alumina with particle sizes of 0.3, 0.1, and 0.05 µm. The polished X-sections were then rinsed in flowing water and etched for 30 seconds to expose the X-section microstructure of the treated layers under OM. A mixture of acetic acid (50 ml), nitric acid (50 ml), and distilled water (30 ml) were used as the etching solution. Finally, a Vickers microhardness tester and optical imaging determined and confirmed the treated layer thickness. Additionally, several characterization devices were employed to investigate the triple-treated specimens, then the results were compared with those from samples that had just been nitrided and annealed. A GDOS technique was used to obtain depth profiles of elemental concentrations in the samples. Analyzing the structure required the use of a diffractometer equipped with Cr radiation. The surface morphology of the treated specimens was examined using SEM. The treated-samples surface was tested for Vickers microhardness at RT with a 100 g load.

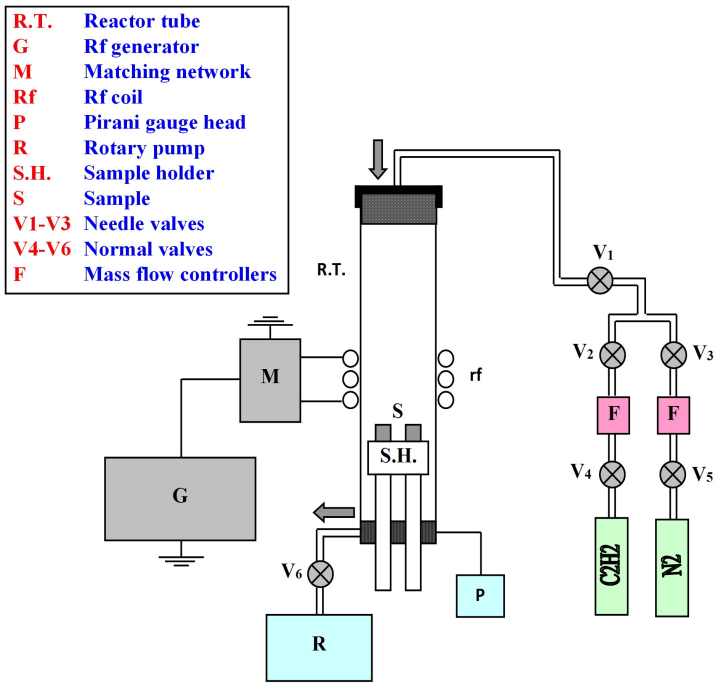

Fig. 1: Schematic diagram of the RF plasma system

3 Results and discussion

3.1 Elemental concentration depth profiles

GDOS was used to study the elemental concentration depth distribution of prenitrided and triple-treated specimens under various C_2H_2 partial pressure ratios. Figs. 2, 3, 4, and 5 reveal the elemental depth profiles of N_2, H_2, O_2, and C respectively, for the differently treated samples. Nitrogen can be discovered in the nitrided layer's studied depth in the prenitrided sample (Fig. 2). The N_2 concentration value is detected to be ~19 at.% near the surface region (N_2 supersaturation region). There is a slight reduction in N_2 concentration with depth in the vicinity of the surface (a few microns down). Behind this, it creates a saturation region of ~11 at.% concentration that extends for ~17 µm in-depth, and then dramatically decreases at the end of the nitrided layer.

Moving from the prenitrided sample to the triple-treated samples, Fig. 2 displays that as the C_2H_2 partial pressure ratio is raised the N_2 supersaturation region is slightly shrunk from ~16 at 10% C_2H_2 to ~13 at.% at 70% C_2H_2. While with rising the C_2H_2 partial pressure ratio, the saturation region is reduced up to a minimum value of ~7 at.% at 70% C_2H_2. As a

result of the drop in the N_2 partial pressure ratio, there has been a fall in N_2 concentration. Moreover, the mean depth profile of N_2 increased after carbonitriding at 10% C_2H_2/ 90% N_2 compared to the prenitrided sample. After annealing, Compound layer N_2 diffuses into the bulk of the substrate [36,37]. Hence, the N_2 depth profile decreases as the C_2H_2 partial pressure ratio is increased.

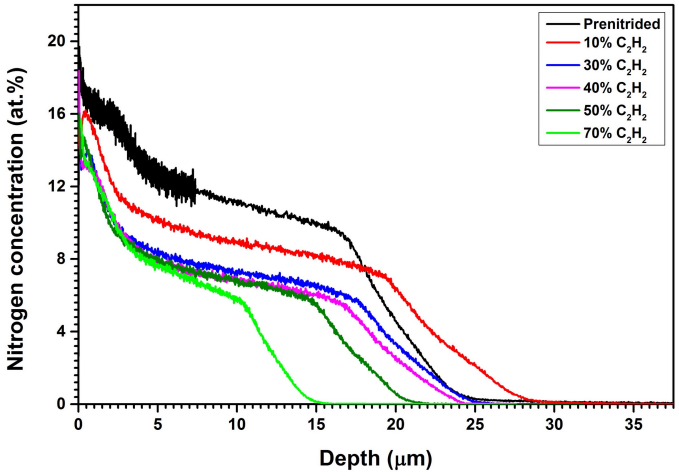

Fig. 2: The nitrogen concentration depth profiles of the prenitrided and triple treated samples at different acetylene gas pressure ratios.

The high temperature during the carbonitriding process causes some nitrided phases to partially decompose, allowing the free N_2 atoms to migrate through the nitride layer toward the bulk sample [11]. The H_2 depth profile for the triple-treated specimens at varied C_2H_2 pressure ratios is also shown in Fig. 3. The H_2 content in the prenitrided sample is so low that it is undetectable. By and large, the H_2 concentrations are generally low, in the range of 10^{-6} at.%. However, its saturation region increases from around 4.15×10^{-6} at.% at 10% C_2H_2 to 5.8×10^{-6} at.% at 70% C_2H_2. The concentration of H_2 increases with depth, forming a saturation region. This saturation region stretches from ~22 μm at 10% C_2H_2 to ~12 μm at 70% C_2H_2. Following that, the saturation region is slightly reduced at the nitride layer's termination. This behavior is analogous to that of the N_2 depth profile. Additionally, Fig. 4 illustrates the elemental depth profile of O_2 in prenitrided and triple-treated specimens at a variety of C_2H_2 pressure ratios. This O_2 concentration is detected due to the residual oxygen contamination in the reactor tube [38]. The O_2 concentration on the surface is ~0.34 at.% for the prenitrided specimen and drops to ~0.06 at.% when the C_2H_2 pressure ratio is increased to 70%. The existence of active hydrogen plasma species that take away the oxide layer from the nitrided layer's surface, could explain this drop. However, the O_2 depth increases from ~0.6 μm following prenitriding to ~1.3 μm following carbonitriding at 40% C_2H_2 and, hence, declines to ~0.4 μm at 70% C_2H_2. This depth is negligible in comparison to the compound layer's thickness, around 3.7%. The thick carbon-rich layer that forms at high C_2H_2 partial pressure ratios hinders further diffusion of N_2, H_2, and O_2 into the compound layer, where the majority of micro-cracks are filled and blocked reactive species such as C and N_2 [39]. As a result, the compound layer becomes thicker (Section 3.4), while the N_2 content declines to a level that can no longer be detected.

On the other hand, Fig. 5 displays the prenitrided sample with two identified C peaks; one near the surface of the nitride layer and another, with a concentration of 0.9 at.%, close to the end of the nitride layer. This C content is identified as a result of contamination of the reactor tube with carbon (residual hydrocarbon gases) [38], where the C atoms can diffuse more quickly in ASS than N_2 atoms [40]. As the partial pressure ratio of C_2H_2 increases, the C concentration on the surface steadily rises to a maximum of 40% C_2H_2 and then slightly declines. It is also worth noting that for all carbonitrided samples, the C depth profile rises immediately below the surface to ~8.6 μm compared to the previous nitrided sample (~2.5 μm). An increased C_2H_2 partial pressure ratio leads to a condenser and thicker carbonitride layer [41]. This partially explains why N_2 mean depth profile is decreasing by increasing the partial pressure ratio of C_2H_2, where N_2 species can diffuse into the sample surface's tiny cracks and grain boundaries [13] under the influence of the N_2 concentration gradient [42]. Furthermore, it is observed that the second C peak rises to a higher depth after carbonitriding at 10% C_2H_2 compared to the prenitrided sample, hence, it goes to a lower depth by increasing the partial pressure ratio of C_2H_2. Again, this is could be attributed to the thick carbon-rich layer formed at high C_2H_2 partial pressure ratios hindering additional diffusion of C and N_2 into the compound layer. In addition, the intensity of that second C peak is 0.7 – 0.84 at.% for the carbonitrided samples from 10% up to 50% C_2H_2, while it increases to 1.28 at.% at the high C_2H_2 partial pressure ratio of 70%. The distribution mechanisms of C and N_2 in ASS have been investigated and interpreted somewhere else [26,43].

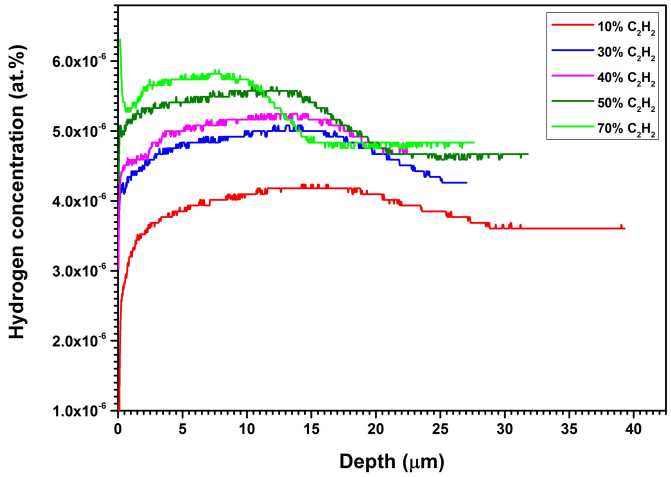

Fig. 3: The hydrogen concentration depth profiles of the triple treated samples at different acetylene gas pressure ratios.

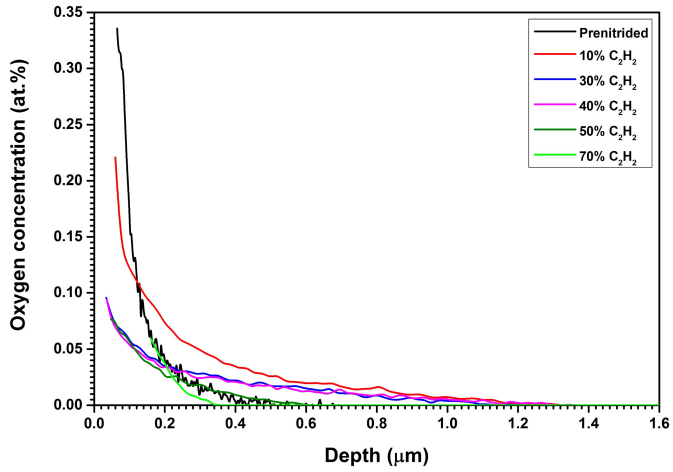

Fig. 4: The oxygen concentration depth profiles of the prenitrided and triple treated samples at different acetylene gas pressure ratios.

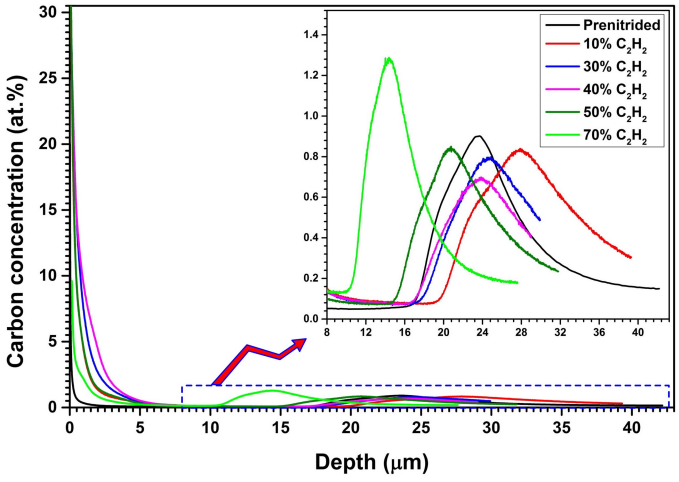

Fig. 5: The carbon concentration depth profiles of the prenitrided and triple treated samples at different acetylene gas pressure ratios.

3.2 Microstructural analysis

XRD was used to determine the crystallographic phases and preferred orientations in the treated samples. Fig. 6 shows the XRD patterns of the prenitrided and triple-treated specimens at varied C_2H_2 partial pressure ratios (10%, 30%, 50%, and 70%).

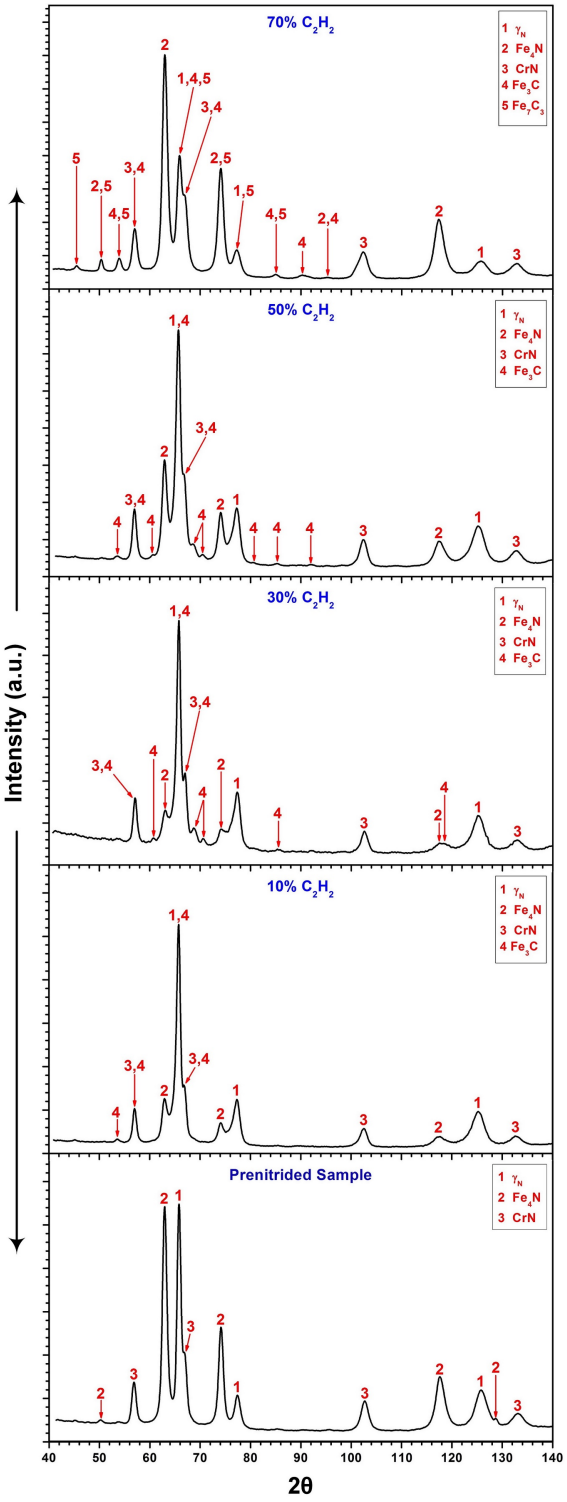

Fig. 6: X-ray diffraction patterns of the prenitrided and carbonitrided samples at different acetylene gas pressure ratios 10%, 30%, 50%, and 70%.

The XRD pattern of the prenitrided specimen demonstrates that the nitride layer is mainly formed of γ_N. The implantation of energetic N_2 ions into the interstitial locations of the ASS matrix can interpret this lattice expansion. However, the lattice expansion is low (~2.6%) where the plasma processing temperature is comparatively high (450 ˚C) and the plasma processing time is only 10 minutes; this results in decreased N_2 inclusion in ASS. Normally, γ_N-phase lattice expansion is inversely dependent on the treating temperature; at 400 ˚C and 465 ˚C, a lattice expansion of 13% and 6.7% was noticed, respectively [44,45]. Moreover, some N_2 content was dissipated in the growth of other detected nitrided phases, such as the $\acute{\gamma}$-Fe_4N and CrN nitrided phases.

It is unlikely that the phase is γ-austenite because there is no substantial change in its intensity along with the treated samples, in spite of the thick modified layer. Consequently, it's most likely this is the γ_N-phase with lattice expansion as little as ~2.6%. The reflection of CrN peaks is quite strong, in agreement with previous investigations of ASS nitrided at similar temperatures [46,47]. CrN formation is preferred because of the low Cr diffusion and high negative enthalpy [48]. Precipitation of the CrN phase in the γ_N-phase matrix is high when the nitriding temperature of ASSs is higher than 450 ˚C, which decreases the matrix Cr content and, hence, a considerable reduction in the corrosion resistance [49]. The large concentration of γ′-Fe_4N in the phase distribution suggests that the surface N_2 potential is high enough to produce higher nitride phases [37]. However, the prenitrided sample does not reveal the γ_C-phase because of a lack of C content in the near-surface section. As the lattice expansion value is so modest, the overlap between γ_N, γ_C, and γ-austenite phases peaks is not ruled out. After carbonitriding, the XRD patterns of triple-treated samples show an extra detectable phase of Fe_3C. Compared to the prenitrided sample, the relative intensity of the γ_N-phase in the triple-treated samples up to 50% C_2H_2 is slightly higher. This might be ascribed to additional N_2 atoms that may have been introduced into the prenitrided layer, but their amount remains tiny, implying that a small lattice expansion has occurred. Furthermore, the 400 ˚C annealing temperature is too low to disperse the γ_N-phase generated during the prenitriding. It's also worth noting that the width of the γ_N-phase peaks is a little wider than the prenitrided sample. An excess of lattice expansion can lead to the appearance of significant compressive stress released over plastic deformation, which increases the surface microhardness of ASS [50,51].

However, its intensity decreases significantly after carbo-nitriding at 70% C_2H_2, where a thick and condensed layer is coated on the sample surface. This thick layer is carbon-rich forming a new carbide phase of Fe_7C_3. In addition, the increase of the C_2H_2 partial pressure ratio raises the treatment temperature further [11], suggesting that dissipation of the γ_N-phase could occur. The $\acute{\gamma}$-Fe_4N phase intensity also decreases following carbonitriding as compared to a prenitrided sample, which is another interesting finding. This may be due to the formation of Fe_3C during carbonitriding. Increasing the C_2H_2 pressure ratio somewhat increases the intensity of the Fe_3C phase, but the overlap between the Fe_3C and CrN phases peaks cannot be ruled out. However, as the partial pressure ratio of C_2H_2 rises to 50% C_2H_2, the intensity of the $\acute{\gamma}$-Fe_4N phase gradually increases, and it sharply increases at 70% C_2H_2. This could be traced back to γ_N-phase dissipation at high carbonitriding temperatures. An increase in the treatment temperature (often above 450 ˚C) can convert the γ_N-phase to other nitrided phases, such as $\acute{\gamma}$-Fe_4N, ε-$Fe_{2-3}N$, CrN, and Cr_2N or martensitic/ferritic phase [52,53]. In the current carbonitriding treatment, increasing the C_2H_2 partial pressure ratio raises the processing temperature from 520 ˚C at 10% C_2H_2 to 590 ˚C at 70% C_2H_2 [11]. Because the CrN and CrC phases have a crystal structure similar to FCC and approximately identical lattice parameters [26], it is difficult to distinguish them. Besides, the triple-treated samples didn't contain enough C atoms to produce the γ_C-phase, so this phase is not detected. Both γ_C and CrC phases can be formed at 100% C_2H_2 treatment [26]. In addition, the residual partial pressure of oxygen is too low to produce metallic oxide or oxynitride phases through nitriding. Carbonitriding may also take away the remaining oxide layer from the nitrided layer due to the presence of active hydrogen species.

3.3 Surface Morphology

Prenitrided and triple-treated specimens of various C_2H_2 pressure ratios (10%, 20%, 30%, 40%, 50%, and 70%) were investigated by SEM at 3000x magnification for the surface morphology (Fig. 7). Figure 7(a) shows the pretreatment sample's surface with relatively large grain size and non-uniform grains with very thin borders, which are distinct features. Normally, the annealing process after nitriding increases the sample grain size [37], this effect can be observed in the triple-treated samples at 10% and 20% C_2H_2 pressure ratios. However, as the C_2H_2 partial pressure ratio rises from 30% to 70%, grain size falls and grain boundaries thicken and densify. A near-linear relationship has been detected between the grain boundary density and the microhardness [54]. Additional tiny deposits on the triple-treated samples could be attributable to amorphous carbonitride films that are hard to identify by XRD analysis. In addition, the surface is porous in microstructure as the grains are randomly packed. Additionally, the surface morphological micro-graphs of the triple-treated samples show a slip between the nearest layers, which is attributed to the increased N_2/C concentration in some places compared to others [11]. As a result, the neigh-boring grains are subjected to compressive stresses, resulting in plastic deformation of the surface [55]. Nitrided surfaces have shown similar features in prior research [11,12,56].

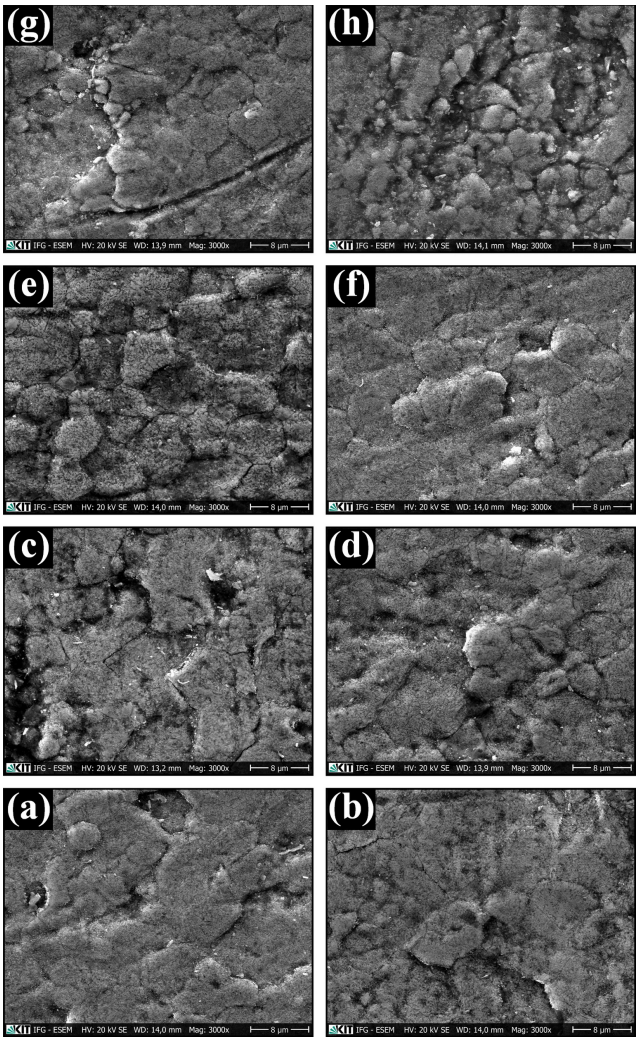

Fig. 7: SEM micrograph of (a) prenitrided sample and triple treated samples at different gas pressure ratios of $C_2H_2/(C_2H_2+N_2)$: (b) 10%, (c) 20%, (d) 30% (e) 40% (f) 50%, (g) 60%, and (h) 70%.

3.4 Cross-section morphological analysis

OM images of the X-section microstructure of prenitrided, annealed-nitrided, and triple-treated specimens at varied C_2H_2 pressure ratios are shown in Fig. 8. After nitriding, Fig. 8(a) reveals that a layer of roughly 20±0.5 µm thick was created on top of the substrate. When it comes to the bulk substrate, it's nearly uniform and homogenous, with a sharp and smooth edge. This thick compound layer was created without eliminating the native oxide layer on the surface. The small oxide layer does not prevent the N_2 diffusion into the bulk-forming a relatively thick modified layer [57]. This confirms that ASS nitriding and carbonitriding are achievable under these conditions of RF plasma treatment [26]. The large compound layer thickness could be ascribed to steel's strong N_2 diffusivity compared to other alloys such as vanadium alloys.

The temperature of thermal diffusion activation of N_2 in ASS is comparatively low (~450 ˚C) [58]. However, it's difficult to see a diffusion layer because of the incredibly short plasma nitriding duration (only 10 min). Annealing for 1 hour at 400 ˚C led to a considerable rise in the thickness of the compound layer from 20 to 23.5±0.5 µm, as shown in Fig. 8(b). Previous research supports this result [37]. Thermal treatment (annealing) has a significant effect on the compound layer's thickness increase through the process of N_2 atoms diffusing toward the substrate bulk. Through this N_2 atom diffusion, the interlayer connection remains intact [59], reflecting the significance of prenitriding prior to carbonitriding. As a result, the N_2 concentration is reduced in the compound layer, therefore, more N_2 atoms may diffuse during the carbonitriding process. Moreover, the surface roughness of the nitrided-annealed sample has been measured via a Form Talysurf Intra Profilometer, reaching 0.256 µm. This value is far less compared to carbonitriding samples (from 2.4 to 7.5 µm), indicating good adhesion between the deposited layer and the annealed-nitrided substrate [59]. A series of micrographs are shown in Fig. 8(c-i), which reveal the carbonitrided layers' deposition after carbonitriding.

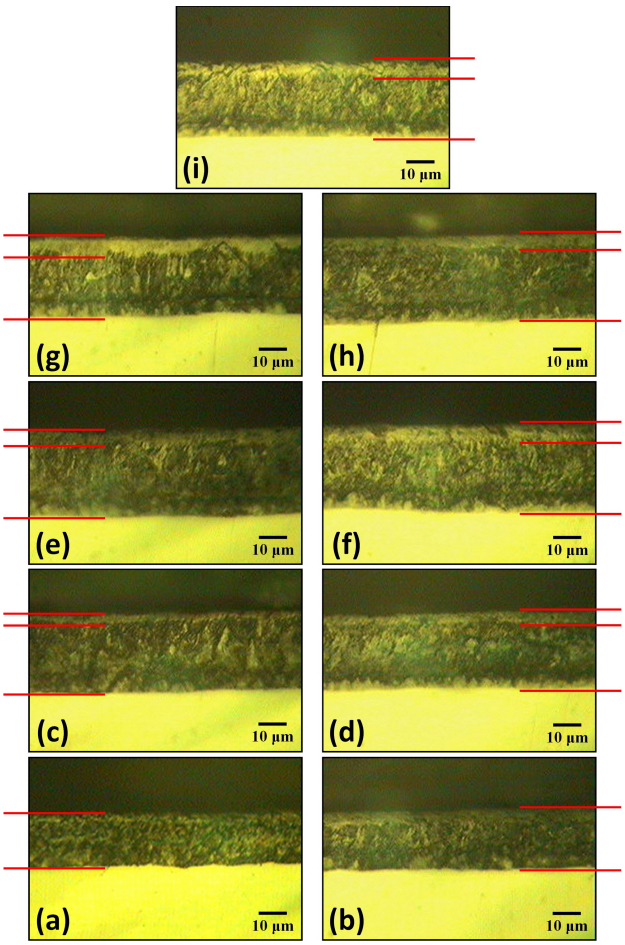

Fig. 8: Cross-sectional OM micrographs of (a) nitrided sample, (b) nitrided-annealed sample and triple treated samples at different gas pressure ratios $C_2H_2/(C_2H_2+N_2)$: (c) 10%, (d) 20%, (e) 30%, (f) 40%, (g) 50%, (h) 60%, and (i) 70%.

Table 1: The total compound thickness and the deposited layer thickness of treated samples.

No.	Gas pressure ratios	Total thickness (µm)	Thickness of deposited layer (µm)
1	Nitrided sample	20 ± 0.5	—
2	Nitrided-annealed sample	23.5 ± 0.5	—
3	10% C_2H_2	30.5 ± 0.5	2.4
4	20% C_2H_2	30.5 ± 0.5	3.9
5	30% C_2H_2	33.5 ± 0.75	4.3
6	40% C_2H_2	34.5 ± 0.75	6.5
7	50% C_2H_2	32.5 ± 0.75	7.5
8	60% C_2H_2	34.5 ± 0.5	5.7
9	70% C_2H_2	31 ± 0.5	7.5

This implies that the deposition mechanism accompanies the surface treatment mechanism, producing an amorphous carbonitride layer on/in the compound layer [11]. In addition, the thickness of the deposition steadily grew from 2.4 to 7.5 µm with an increase in C_2H_2 partial pressure ratio from 10% to 70%, and the treatment temperature increased accordingly. The thickness of the deposited layers was measured via a Vickers microhardness tester and it was found that it is an C_2H_2 partial pressure ratio dependent [41]. For various C_2H_2 partial pressure ratios, the thickness of the compound and deposited layers is summarized in Table 1. According to Fig. 8 and Table 1, the compound layer thickness enlarged from 25.5 µm to about 29 µm after carbonitriding at 60% C_2H_2. Nitrogen diffusion acceleration toward the substrate bulk beneath the nitride layer might be aided by a gradient of N_2/C concentration in addition to a temperature gradient [38].

3.5 Microhardness

A Vickers microhardness tester with 100 g weight and a 15 sec hold period was used to investigate the impact of various C_2H_2 pressure ratios on the surface hardness. Fig. 9 displays the surface microhardness values of the prenitrided, nitrided-annealed, and triple-treated specimens. The prenitrided sample has a surface microhardness of 1,051 HV0.1 that is roughly 4.78 times greater than the untreated sample value (220 HV0.1).

Due to the creation of γ′-Fe_4N and γ_N hard phases, surface hardness has increased [11]. The γ_N-phase has varying high microhardness over a large range of about 1,000–2,000 HV [60,61,62]. The variation in properties of the γ_N-phase is attributed to its complex states and its different microstructures on the nitrided surfaces of ASSs [53]. The surface hardness is reduced to 822 HV0.1 after heat treatment (annealing at 400 ˚C). Due to the drop in dislocation density and a raise in grain size, this decrease could be demonstrated [63,64]. Nitrogen atoms are also diffusing out of the compound layer, increasing its thickness from ~20 to ~23.5 µm and releasing the compressive stress. It is important to note, however, that this hardness value is sufficient to prevent plastic deformation from removing the carbonitrided layer, as long as the soft substrate material is reduced [65]. After carbonitriding, all triple-treated samples show a hardness improvement compared to the nitrided-annealed sample. The highest value of surface hardness, 1,497±33.5 HV0.1, can be achieved by increasing the C_2H_2/N_2 gas composition ratio to 70%. When compared to the untreated and prenitrided samples, this maximum hardness value is ~6.8 and ~1.42 times higher. This maximum value is higher than that value (1,356±12 HV0.1), which we have achieved earlier by duplex plasma treatment (nitriding then carbonitriding) without annealing in between [17]. This increase is attributed to six factors: 1) an increase in the hard deposit layer thickness [66]; 2) a dense microstructure of the carbonitride layer with high N_2 and C concentrations near the surface and along the saturation region; 3) a rise in the intensity of γ′-Fe_4N hard nitride phase; 4) forming Fe_3C and Fe_7C_3 hard carbide phases that add more internal stress to the treated layer; 5) forming the γ_N hard phase but the softer γ_C-phase is no [40]; and finally 6) decreasing the grain size [64] with increasing the C_2H_2 partial pressure ratio.

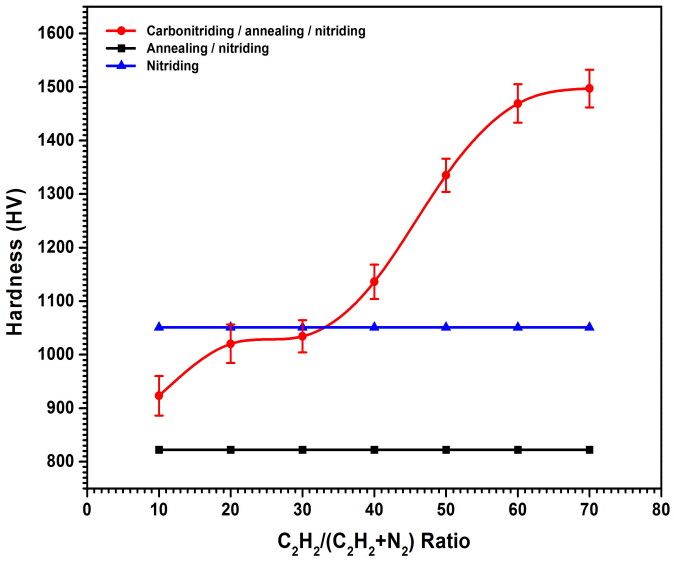

Fig. 9: The surface microhardness of the treated samples versus gas pressure ratios.

4 Conclusion

To our knowledge, this is the first time that ASS has been subjected to such a triple treatment. The C_2H_2/ N_2 gas ratio was studied to determine how the annealed-plasma nitrided samples of AISI 304 were affected. There is an association between the gas composition and changes in the triple-treated layers' thickness, atomic structure, chemical composition as well as microhardness values. The microstructures of the triple-treated samples show the formation of hard phases of γ_N, γ'-Fe_4N, CrN, Fe_3C, and Fe_7C_3. The overall compound layer thickness raised from ~20 µm after nitriding to ~23.5 µm after annealing to ~34.5 µm after carbonitriding. Moreover, the mean depth profile of N_2 decreases as the partial pressure ratio of C_2H_2 increases from 10% to 70%. An amorphous carbonitride film has been formed on the top layer of the triple-treated samples leading to fine precipitations. The deposited top layer has a maximum thickness of ~7.5 µm at 70% C_2H_2 and it is gas composition dependent. There was an increase of ~6.8 and ~1.42 folds in the surface microhardness of the triple-treated sample at 70% C_2H_2 compared to the untreated and prenitrided samples, respectively.

Acknowledgment:

The authors are grateful to Dr. L. Pichon and Dr. C. Timplier at Poitiers University in France for contributing some facilities for evaluating the samples. The authors acknowledge the Academy of Scientific Research and Technology-Egypt for the financial support in the framework of the science up faculty of science program. Grant No. 6645.

Conflict of interest

The authors declare that there is no conflict regarding the publication of this paper.

References

[1] Abedi HR, Salehi M, Yazdkhasti M, Hemmasian-E A (2010) Effect of high temperature post-oxidizing on tribological and corrosion behavior of plasma nitrided AISI 316 austenitic stainless steel. Vacuum, **(85)**, 443–447. https://doi.org/10.1016/j.vacuum.2010.08.008

[2] López-Ojeda L, Vargas-Gutiérrez G (2022) High wear resistance and better pitting corrosion resistance of AISI 316L stainless steel by a self-protective oxy-nitrocarburizing paste. Journal of Materials Research and Technology, **(16)**, 1803–1813. https://doi.org/10.1016/j.jmrt.2021.12.118

[3] Moghadasi K, Mohd Isa MS, Ariffin MA, et al (2022) A review on biomedical implant materials and the effect of friction stir based techniques on their mechanical and tribological properties. Journal of Materials Research and Technology, **(17)**, 1054–1121. https://doi.org/10.1016/j.jmrt.2022.01.050

[4] Chen YY, Liou YM, Shih HC (2005) Stress corrosion cracking of type 321 stainless steels in simulated petrochemical process environments containing hydrogen sulfide and chloride. Materials Science and Engineering: A **(407)**, 114–126. https://doi.org/10.1016/j.msea.2005.07.011

[5] Mukhopadhyay CK, Jayakumar T, Raj B, Ray KK (2000) The influence of notch on the acoustic emission generated during tensile testing of nuclear grade AISI type 304 stainless steel. Materials Science and Engineering: A, **(276)**, 83–90. https://doi.org/10.1016/S0921-5093(99)00512-2

[6] Collins GA, Hutchings R, Tendys J (1991) Plasma immersion ion implantation of steels. Materials Science and Engineering: A, **(139)**, 171–178. https://doi.org/10.1016/0921-5093(91)90613-R

[7] Sato S, Arai Y, Yamashita N, et al (2012) Surface-nitriding treatment of steels using microwave-induced nitrogen plasma at atmospheric pressure. Applied Surface Science, **(258)**, 7574–7580. https://doi.org/10.1016/j.apsusc.2012.04.090

[8] Zhao X-Q, Zhou H-D, Chen J-M (2006) Comparative study of the friction and wear behavior of plasma sprayed conventional and nanostructured WC–12%Co coatings on stainless steel. Materials Science and Engineering: A, **(431)**, 290–297. https://doi.org/10.1016/j.msea.2006.06.009

[9] Araújo AGF, Naeem M, Araújo LNM, et al (2020) Design, manufacturing and plasma nitriding of AISI-M2 steel forming tool and its performance analysis. Journal of Materials Research and Technology, **(9)**, 14517–14527. https://doi.org/10.1016/j.jmrt.2020.10.048

[10] El-Hossary F., Negm N., Khalil S., Abd Elrahman A. (2002) Formation and properties of a carbonitrided layer in 304 stainless steel using different radio frequency plasma powers. Thin Solid Films, **(405)**, 179–185. https://doi.org/10.1016/S0040-6090(01)01729-1

[11] El-Hossary FM, Negm NZ, Abd El-Rahman AM, Hammad M (2009) Duplex treatment of 304 AISI stainless steel using rf plasma nitriding and carbonitriding. Materials Science and Engineering: C 29:1167–1173. https://doi.org/10.1016/j.msec.2008.09.049

[12] El-Hossary FM, Negm NZ, El-Rahman AMA, et al (2008) Duplex treatment of AISI 304 austenitic stainless steel using rf nitriding and dc reactive magnetron sputtering of titanium. Surface and Coatings Technology, **(202)**, 1392–1400. https://doi.org/10.1016/j.surfcoat.2007.06.066

[13] El-Hossary F. (2002) The influence of surface microcracks and temperature gradients on the rf plasma nitriding rate. Surface and Coatings Technology, **(150)**, 277–281. https://doi.org/10.1016/S0257-8972(01)01524-9

[14] Shen D-J, Wang Y-L, Nash P, Xing G-Z (2007) A novel method of surface modification for steel by plasma electrolysis carbonitriding. Materials Science and Engineering: A, **(458)**, 240–243. https://doi.org/10.1016/j.msea.2006.12.067

[15] Morita T, Hirano Y, Asakura K, et al (2012) Effects of plasma carburizing and DLC coating on friction-wear characteristics, mechanical properties and fatigue strength of stainless steel. Materials Science and Engineering: A, **(558)**, 349–355. https://doi.org/10.1016/j.msea.2012.08.011

[16] Lei MK, Zhang ZL (1997) Microstructure and corrosion resistance of plasma source ion nitrided austenitic stainless steel. Journal of Vacuum Science & Technology A: Vacuum, Surfaces, and Films, **(15)**, 421–427. https://doi.org/10.1116/1.580501

[17] Rozendaal HCF, Colijn F, Mittemeijer EJ (1985) Morphology, Composition, and Residual Stresses of Compound Layers of Nitrocarburized Iron and Steels. Surface Engineering, **(1)**, 30–42. https://doi.org/10.1179/sur.1985.1.1.30

[18] E. J. Mittemeijer, H. C. F. Rozendaal, P. F. Colijn PJVDS andR. TF (1981) Proceedings of the Conference on Heat Treatment. The Metals Society, London, Birmingham UK

[19] E. ROLINSKI (1985) ibid. 3:35

[20] Wang J, Xiong J, Peng Q, et al (2009) Effects of DC plasma nitriding parameters on microstructure and properties of 304L stainless steel. Materials Characterization, **(60)**, 197–203. https://doi.org/10.1016/j.matchar.2008.08.011

[21] Z. L. ZHANG and T. BELL (1985) ibid. 1:131

[22] P.A. Dearnley, A. Namver, G. G. A. Hibberd and T. Bell, in: E. Broszeit, W.D. Munz, H. Oechsner, K.-T. Rie GKW (1989) DGM Informationsgesellschaft, Oberursel, “Proceedings of the 1st International Conference on Plasma Surface Engineering, Garmisch – Partenkirchen". In: Plasma-Surface Engineering. pp 219–226

[23] Gemma K, Satoh Y, Ushioku I, Kawakami M (1995) Abnormal nitriding behaviour of a high chromium, high manganese austenitic steel. Surface Engineering, **(1)**, :240–245. https://doi.org/10.1179/sur.1995.11.3.240

[24] Samandi M (1994) Significance of nitrogen mass transfer mechanism on the nitriding behavior of austenitic stainless steel. Journal of Vacuum Science & Technology B: Microelectronics and Nanometer Structures, **(12)**, 935. https://doi.org/10.1116/1.587331

[25] Ibrahim K, Rahman MM, Zhao X, et al (2018) Annealing effects on microstructural, optical, and mechanical properties of sputtered CrN thin film coatings: Experimental studies and finite element modeling. Journal of Alloys and Compounds, **(750)**, 451–464 https://doi.org/10.1016/j.jallcom.2018.04.012

[26] Abd El-Rahman AM, El-Hossary FM, Fitz T, et al (2004) Effect of N2 to C2H2 ratio on r.f. plasma surface treatment of austenitic stainless steel. Surface and Coatings Technology, **(183)**, 268–274. https://doi.org/10.1016/j.surfcoat.2003.09.057

[27] Zhang ZL, Bell T (1985) Structure and Corrosion Resistance of Plasma Nitrided Stainless Steel. Surface Engineering, **(1)**, 131–136. https://doi.org/10.1179/sur.1985.1.2.131

[28] Blawert C, Mordike BL, Collins GA, et al (2000) Characterisation of duplex layer structures produced by simultaneous implantation of nitrogen and carbon into austenitic stainless steel X5CrNi189. Surface and Coatings Technology, **(128–129)**, 219–225. https://doi.org/10.1016/S0257-8972(00)00651-4

[29] Dalibón EL, Czerwiec T, Trava-Airoldi VJ, et al (2019) Characterization of DLC coatings over nitrided stainless steel with and without nitriding pre-treatment using annealing cycles. Journal of Materials Research and Technology, **(8)**, 1653–1662. https://doi.org/10.1016/j.jmrt.2018.12.002

[30] Zhao C, Sun D, Hou J (2007) Duplex treatments of plasma nitrocarburizing and post-oxidation in an adiabatic plasma furnace. Surface and Coatings Technology, **(201)**, 4984–4986. https://doi.org/10.1016/j.surfcoat.2006.07.084

[31] Van Stappen M, Malliet B, Stals L, et al (1991) Characterization of TiN coatings deposited on plasma nitrided tool steel surfaces. Materials Science and Engineering: A, **(140)**, 554–562. https://doi.org/10.1016/0921-5093(91)90478-6

[32] Abedi HR, Salehi M, Yazdkhasti M (2010) Novel plasma nitriding–oxidizing duplex treatment of AISI 316 austenitic stainless steel. Materials Letters, **(64)**, 698–701. https://doi.org/10.1016/j.matlet.2009.12.042

[33] Gavriljuk V. G.; Berns H. (1999) High Nitrogen Steels Gavriljuk V. G., Berns H. Springer-Verlag, Berlin

[34] Pawlowski L (2008) The Science and Engineering of Thermal Spray Coatings, 2nd Editio. John Wiley & Sons, New York

[35] Zhang J, He Y, Wang Y, et al (2019) Influence of annealing temperature on microstructure, tensile properties and tensile deformation mechanism of metastable austenitic stainless steel repetitively cold-rolled and annealed. Materialia, **(8)**, 100455.

https://doi.org/10.1016/j.mtla.2019.100455

[36] Louro C, Cavaleiro A, Dub S, et al (2002) The depth profile analysis of W-Si-N coatings after thermal annealing. Surface and Coatings Technology, **(161)**, 111–119. https://doi.org/10.1016/S0257-8972(02)00325-0

[37] Negm NZ (2006) Effect of annealing temperature on properties of H2/N2 rf plasma-treated stainless steel. Surface and Coatings Technology, **(201)**, 1763–1767. https://doi.org/10.1016/j.surfcoat.2006.03.003

[38] Czerwiec T, He H, Weber S, et al (2006) On the occurrence of dual diffusion layers during plasma-assisted nitriding of austenitic stainless steel. Surface and Coatings Technology, **(200)**, 5289–5295. https://doi.org/10.1016/j.surfcoat.2005.06.014

[39] El-Hossary FM, Negm NZ, Khalil SM, et al (2001) RF plasma carbonitriding of AISI 304 austenitic stainless steel. Surface and Coatings Technology, **(141)**, 194–201. https://doi.org/10.1016/S0257-8972(01)01036-2

[40] Blawert C, Kalvelage H, Mordike B., et al (2001) Nitrogen and carbon expanded austenite produced by PI3. Surface and Coatings Technology, **(136)**, 181–187. https://doi.org/10.1016/S0257-8972(00)01050-1

[41] Hao J, Liu W, Xue Q (2007) Effect of N2/CH4 flow ratio on microstructure and composition of hydrogenated carbon nitride films prepared by a dual DC-RF plasma system. Journal of Non-Crystalline Solids, **(353)**, 136–142. https://doi.org/10.1016/j.jnoncrysol.2006.10.008

[42] Tibbetts GG (1974) Role of nitrogen atoms in ``ion-nitriding''. Journal of Applied Physics, **(45)**, 5072–5073. https://doi.org/10.1063/1.1663186

[43] da Silva JRG, McLellan RB (1976) Diffusion of carbon and nitrogen in B.C.C. iron. Materials Science and Engineering, **(26)**, 83–87. https://doi.org/10.1016/0025-5416(76)90229-9

[44] Mändl S, Scholze F, Neumann H, Rauschenbach B (2003) Nitrogen diffusivity in expanded austenite. Surface and Coatings Technology, **(174–175)**, 1191–1195. https://doi.org/10.1016/S0257-8972(03)00454-7

[45] Liang W (2003) Surface modification of AISI 304 austenitic stainless steel by plasma nitriding. Applied Surface Science, **(211)**, 308–314. https://doi.org/10.1016/S0169-4332(03)00260-5

[46] Sundararaman D, Kuppusami P, Raghunathan VS (1987) A study of plasma-nitrided AISI type 316 stainless steel. Surface and Coatings Technology, **(30)**, 343–354. https://doi.org/10.1016/0257-8972(87)90126-5

[47] Abd El-Rahman AM, Negm NZ, Prokert F, et al (2005) Depth-related microstructure of rf plasma nitrocarburized austenitic stainless steel. Surface and Coatings Technology, **(191)**, 140–147. https://doi.org/10.1016/j.surfcoat.2004.03.053

[48] Foerster CE, Souza JFP, Silva CA, et al (2007) Effect of cathodic hydrogenation on the mechanical properties of AISI 304 stainless steel nitrided by ion implantation, glow discharge and plasma immersion ion implantation. Nuclear Instruments and Methods in Physics Research Section B: Beam Interactions with Materials and Atoms, **(257)**, 727–731. https://doi.org/10.1016/j.nimb.2007.01.267

[49] Shen L, Wang L, Wang Y, Wang C (2010) Plasma nitriding of AISI 304 austenitic stainless steel with pre-shot peening. Surface and Coatings Technology, **(204)**, 3222–3227. https://doi.org/10.1016/j.surfcoat.2010.03.018

[50] Wilbur PJ, Davis JA, Wei R, et al (1996) High current density, low energy, ion implantation of AISI-M2 tool steel for tribological applications. Surface and Coatings Technology, **(83)**, 250–256. https://doi.org/10.1016/0257-8972(95)02830-7

[51] Riviere J., Meheust P, Villain J., et al (2002) High current density nitrogen implantation of an austenitic stainless steel. Surface and Coatings Technology, **(158–159)**, 99–104. https://doi.org/10.1016/S0257-8972(02)00227-X

[52] Blawert C, Mordike BL, Jirásková Y, Schneeweiss O (1999) Structure and composition of expanded austenite produced by nitrogen plasma immersion ion implantation of stainless steels X6CrNiTi1810 and X2CrNiMoN2253. Surface and Coatings Technology, **(116–119)**, 189–198. https://doi.org/10.1016/S0257-8972(99)00086-9

[53] Lei MK (1999) Phase transformations in plasma source ion nitrided austenitic stainless steel at low temperature. Journal of Materials Science, **(34)**, 5975–5982. https://doi.org/https://doi.org/10.1023/A:1004728711459

[54] Wang J, Hong H, Huang A, et al (2022) New insight into the relationship between grain boundaries and hardness in bainitic/martensitic steels from the crystallographic perspective. Materials Letters, **(308)**, 131105. https://doi.org/10.1016/j.matlet.2021.131105

[55] Borgioli F, Fossati A, Galvanetto E, Bacci T (2005) Glow-discharge nitriding of AISI 316L austenitic stainless steel: influence of treatment temperature. Surface and Coatings Technology, **(200)**, 2474–2480. https://doi.org/10.1016/j.surfcoat.2004.07.110

[56] Liang W, Xiaolei X, Jiujun X, Yaqin S (2001) Characteristics of low pressure plasma arc source ion nitrided layer on austenitic stainless steel at low temperature. Thin Solid Films, **(391)**, 11–16. https://doi.org/10.1016/S0040-6090(01)00969-5

[57] Figueroa CA, Alvarez F (2005) New pathways in plasma nitriding of metal alloys. Surface and Coatings Technology, **(200)**, 498–501. https://doi.org/10.1016/j.surfcoat.2005.02.089

[58] García JA, Fuentes GG, Martínez R, et al (2004) Temperature-dependent tribological properties of low-energy N-implanted

V5Ti alloys. Surface and Coatings Technology, **(188–189)**, 459–465. https://doi.org/10.1016/j.surfcoat.2004.08.053

[59] Chowdhury AKM., Cameron D., Hashmi MS. (1999) Adhesion of carbon nitride thin films on tool steel. Surface and Coatings Technology, **(116–119)**, 46–53. https://doi.org/10.1016/S0257-8972(99)00317-5

[60] Kazuo Ichii, Kimio Fujimura TT (1986) Structure of ion nitrided layers of 18-8 stainless steel. Technology Reports of Kansai University, **(27)**, 135–144

[61] Menthe E, Rie K-T, Schultze JW, Simson S (1995) Structure and properties of plasma-nitrided stainless steel. Surface and Coatings Technology, **(74–75)**, 412–416. https://doi.org/10.1016/0257-8972(95)08246-8

[62] Williamson DL, Ozturk O, Wei R, Wilbur PJ (1994) Metastable phase formation and enhanced diffusion in f.c.c. alloys under high dose, high flux nitrogen implantation at high and low ion energies. Surface and Coatings Technology, **(65)**, 15–23. https://doi.org/10.1016/S0257-8972(94)80003-0

[63] Mazilkin AA, Straumal BB, Protasova SG, et al (2008) Structure, phase composition, and microhardness of carbon steels after high-pressure torsion. Journal of Materials Science, **(43)**, 3800–3805. https://doi.org/10.1007/s10853-007-2222-5

[64] Lu YH, Wang JP, Tao SL, Zhou ZF (2011) Effect of annealing temperature on microstructure, hardness and adhesion properties of TiSixNy superhard coatings. Applied Surface Science, **(257)**, 6380–6386. https://doi.org/10.1016/j.apsusc.2011.01.128

[65] Sun Y, Bell T (1991) Plasma surface engineering of low alloy steel. Materials Science and Engineering: A, **(140)**, 419–434. https://doi.org/10.1016/0921-5093(91)90458-Y

[66] Fossati A, Borgioli F, Galvanetto E, Bacci T (2006) Glow-discharge nitriding of AISI 316L austenitic stainless steel: influence of treatment time. Surface and Coatings Technology, **(200)**, 3511–3517. https://doi.org/10.1016/j.surfcoat.2004.10.122